Measurement of Monotonic Biaxial Elastoplastic Stresses at Notch Roots

W. N. Sharpe, Jr.
Department of Mechanical Engineering,
The Johns Hopkins University,
Baltimore, MD 21218
Fellow ASME

Biaxial principal strains were measured at the roots of notches in aluminum specimens with a laser-based interferometric technique. Interference patterns from three tiny indentations spaced 150 or 200 micrometers apart in an orthogonal pattern were monitored with a microcomputer-controlled system. Elastoplastic strains up to one percent were measured in real time with a resolution of 25 microstrain. Procedures were developed for computing the two principal stresses from the incremental strain data using J_2-flow theory. The validity of the computations was checked by computing the stresses in smooth tensile specimens. Anisotropy in the thin sheet material leads to errors in the computed lateral stresses (which should be zero), but the maximum deviation of the computed effective stress from the uniaxial stress is only five percent. Three kinds of double-notched specimens were prepared to vary the amount of constraint at the notch root. These were tested under monotonic tensile loading and the biaxial notch-root strains recorded. There is considerable variation among the strains once the elastic limit is passed. This is due primarily to the local inhomogeneity of plastic strain, since the gage length of the measurement is only a few times larger than the grain size of the material. Local biaxial stresses were computed from the measured strains for the three cases. The nature of the material's stress-strain curve tends to smooth out the variations among tests, particularly when the effective stress is computed. It is discovered that the local stress predicted by the Neuber relation agrees very closely with the measured local effective stress.

1 Introduction

The prediction and measurement of stresses and strains at "stress concentrations" is an important problem in the field of solid mechanics. Given the long history of research into the elastic problem and the availability of sophisticated finite element codes, one can expect to get good agreement between predicted and measured elastic stresses and/or strains. However, the situation is not so favorable when the elastic limit of the materials has been exceeded—theories carry restrictive assumptions, computer predictions are cumbersome, and measurements can no longer be made on elastic models such as those used in photoelasticity. Local elastoplastic response at a discontinuity in a component or structure is still a rich area for research from an experimental, theoretical, and computational viewpoint.

The ability to predict stresses (as opposed to strains) is important from design considerations; one is much more likely to know the applied loads than the applied deformations. But of course one does not measure stress directly; one measures load on a simple geometry or measures strains on a complicated geometry. Conversion to stress occurs through the basic definition if load is measured and through the constitutive equations if strains are measured. This latter process is straightforward for elastic behavior, but less well developed for elastoplastic behavior. A major reason is the difficulty of measuring the elastoplastic strains in situations that are truly meaningful. Plasticity tends to initiate at stress concentrations, and in most cases these are relatively small which inhibits the use of the ubiquitous foil gages. Another difficulty with the study of elastoplastic behavior is that one cannot scale up the problem because the material's grain size is so important.

This paper reports the results of a series of experiments on three geometries of double-notched specimens of 2024 aluminum. These three cases were chosen to vary the amount of lateral constraint at the notch root. Longitudinal and lateral strains, ϵ_1 and ϵ_2, were measured at the notch roots with a laser-based technique having a gage length of either 150 μm and 200 μm—only a bit larger than the grain size of the material. These measured principal strains are then converted into stresses using the incremental version of the J_2 theory of plasticity. The material tested is not isotropic which the theory assumes, and this contributes to errors in the computed stresses;

Contributed by the ASME Applied Mechanics Division of THE AMERICAN SOCIETY OF MECHANICAL ENGINEERS for presentation at the Winter Annual Meeting, Atlanta, Georgia, Dec. 1-6, 1991.

Discussion on this paper should be addressed to the Technical Editor, Prof. Leon M. Keer, The Technological Institute, Northwestern University, Evanston, IL 60208, and will be accepted until two months after final publication of the paper itself in the JOURNAL OF APPLIED MECHANICS. Manuscript received by the ASME Applied Mechanics Division, Sept. 7, 1989; final revision, Nov. 26, 1990.

Paper No. 91-WA/APM-5.

however, it is very important technologically because the sheet material is widely used in the skins of aircraft.

The results reported here are part of a larger study of the elastoplastic behavior at notch roots under cyclic loading—the implications are obvious, one wants to be able to predict the initiation of cracks under low-cycle fatigue conditions. The discussion here focuses only the first monotonic part of the loading cycle. The Neuber relation (Neuber, 1961)

$$K_\sigma \times K_\epsilon = K_t^2 \tag{1}$$

(where K_σ is the stress concentration factor, K_ϵ is the strain concentration factor, and K_t is the elastic stress concentration factor) is widely used for predicting the stresses and strains at notch roots. It is generally regarded as satisfactory for plane stress loading, but not for loadings approaching plane strain. Another paper (Sharpe and Wang, 1991) explores this effect of constraint on the validity of a modified version of the Neuber relation for monotonic loading; the predicted strains were compared with the measured ones. The conclusion there is that a modification of the Neuber relation which makes it look more like a linear relation ($K_\epsilon = K_t$) is an improvement when constraints are present.

The development and application of the Neuber relation is reviewed in the Background section of Sharpe and Wang (1991) and will not be repeated here. Surprisingly, there have been few measurements of elastoplastic stresses in complicated geometries; those are reviewed in Section 2 of this paper. The local biaxial strains are measured with a laser-based interferometric technique that measures the relative displacements between three tiny indentations in the specimen surface. The computer-controlled version for measuring uniaxial strain has been described elsewhere (Guillot and Sharpe, 1983) but the important advance reported here is the extension of the system to biaxial measurements of the principal strains ϵ_1 and ϵ_2. The technique is described only briefly since this paper focuses more on the results than on the details of the measurement system.

The procedure for computing the stresses from the measured strains, which is a straightforward inversion of the equations of plasticity, is then presented. These procedures are applied to stress-strain data from smooth specimens (both ϵ_1 and ϵ_2 were measured) to validate the computational procedure and examine the effect of anisotropy.

At this point, one should have confidence in the stress measurements and can move on to the geometries in question. Measured biaxial notch-root strains room the three cases (ten different specimens were tested) are then presented; these serve as the input for the stress calculations. The measured stresses are presented as principal values σ_1 and σ_2. These are used to compute the effective stress σ_e which is compared to the stress predicted by the Neuber relation. Finally, conclusions are drawn as to the significance of the results.

2 Background

Theocaris (1962) wrote a paper in 1962 entitled "Experimental Solution of Elastic-Plastic Plane Problems" in which he presented procedures for computing stresses from strains measured by photoelastic coatings on specimens. He presents the equations for computing the change in stress components $d\sigma_x$, $d\sigma_y$, and $d\tau_{xy}$ from the measured strain increments $d\epsilon_x$, $d\epsilon_y$, and $d\gamma_{xy}$. The specimen was a thin steel sheet with large semicircular double notches to which a thin photoelastic coating was glued. The measurement of strains required analyses of patterns taken at normal and at oblique incidence and was tedious at best; however, it did give the strain field. The incremental theory of plasticity based on J_2 was used, but only seven increments were taken between the load corresponding to incipient plasticity at the notch root and the load corresponding to the spread of plasticity across the net section. McClintock (1963) praised the paper in a later discussion and compared the measured stress and strain concentrations to those predicted by the Neuber relation—showing that the predictions were accurate in the early stages of plastic deformation at the notch root.

A similar work was published shortly thereafter by Durelli and Sciammarella (1963) who measured strains by moiré techniques on a thin aluminum specimen with a central hole. Six load increments were used which required iteration of the stress increments to assure that the effective stress-strain curve was being followed. The stress field in the neighborhood of the hole was measured, and the stress and strain concentrations were compared to those from the classic experimental work by Griffith in 1948. Agreement was excellent, considering the slight difference in specimen materials.

Photoplastic materials with nonlinear behavior similar to that of metals are quite useful in gaining an understanding of the development of plasticity in a given geometry and in evaluating theories. An example of such a study is the fine work by Johnson (1976) in which he studied the plastic deformation of a circumferentially notched shaft subjected to torsion loading. He used a photoplastic material that has a stress-strain curve similar in shape to a medium-strength aluminum and the scattered light technique to measure the stresses on a plane down the center of the shaft. The material was calibrated in torsion, so he determined shear stresses directly from the fringe patterns. The stress and strain concentrations showed good agreement with the Neuber prediction for early stages of yielding; indeed, this geometry is the same as analyzed by Neuber.

One wonders why foil-resistance strain gages are not used to measure the necessary plastic strains; the larger post-yield ones have the capability of measuring strains to ten percent or more. One paper by Keil and Benning (1979) on their use appears in 1979. However, they use the deformation theory of plasticity instead of an incremental theory which, although requiring additional assumptions, is easier to apply. They work only with principal strains and provide nomographs from which one can obtain the stresses for a representative selection of materials. Given two strain measurements, one reads out the two principal stresses.

It appears that the paucity of research papers describing measurements of elastoplastic stresses is due more to the difficulty in measuring the strains than anything else. In fact, the *Handbook on Experimental Mechanics* (1987) presents the equations relating strain increments to stress increments on page 10, but there is no later reference to their actual use. Precedents have been set with the works of Theocaris and of Durelli and Sciammarella, and similar studies would be considerably easier with modern imaging and computational capabilities. However, these earlier works did not measure at the point of real interest—the root of the stress concentration where fatigue cracks initiate.

3 Strain Measurement Technique

The interferometric Strain/Displacement Gage (or ISDG) is a laser-based system that measures in-plane relative displacement between tiny reflective indentations in a specimen surface. The pyramidal-shaped indentations are oriented so that the light rays diffracted from their sides overlap to form interference patterns in space. When the distance between the indents changes, the fringe patterns move; in effect, one simply has an optical lever with a high ratio because of the interference phenomenon. A microcomputer-controlled system for measuring fractional fringe motion has been developed that has suitable resolution for elastoplastic strain measurement over gage lengths as short as 100 μm (Guillot and Sharpe, 1983). For more details about various applications of the technique, see Sharpe (1982).

Strains in two orthogonal directions can be measured if three indentations are placed in the specimen surface as shown in

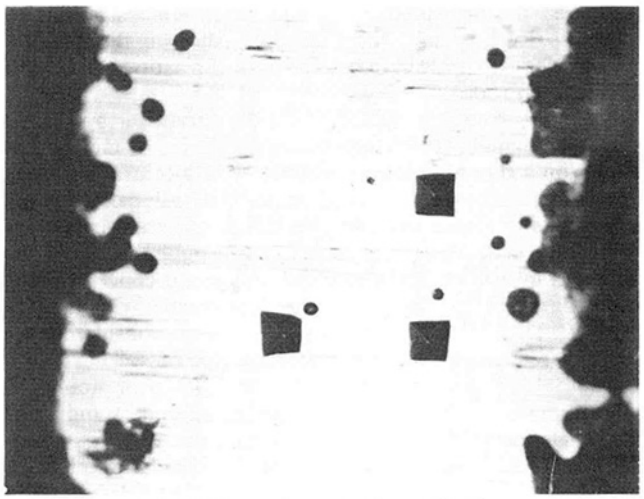

Fig. 1 Three indentations at the root of a notch. The spacing is 150 micrometers, and they are placed at the root of a notch with a 1-mm radius. The black areas on either side are paint that was applied to reduce stray reflections.

Fig. 1. That photomicrograph shows indentations at the root of a notch with a 1-mm radius; the spacing between them is 150 μm. Longitudinal strain is measured in the direct of loading, and lateral strain is measured in the perpendicular direction. The black areas at the sides of Fig. 1 are flat-black paint that was applied to limit stray reflections from the polished specimen surface.

Four fringe patterns are generated with the biaxial ISDG, and one must use four fringe sensors (scanning mirrors and photomultiplier tubes) to monitor the patterns and average out the rigid body motion of the specimen. A microcomputer system monitors the fringe motions, converts them to strains, stores the load and strains, and increments the load control signal to the test machine. The sampling rate is approximately ten points per second, and the least count of strain is approximately 35 microstrain for the 150-μm gage length. The relative uncertainty associated with the measurement of the relative displacement of the indentations is approximately $\pm$ three percent.

The effect of the indentations on the local strain field, especially in the plastic region, is a matter of concern. Unfortunately, there is no other experimental technique with a suitably short gage length, resolution, and range to permit a direct comparison at a notch root. The best that one can do is compare the ISDG with other techniques on smooth specimens, and this is quite good for longitudinal strains as will be seen in Fig. 3. Further, the reproducibility and reasonable behavior of the notch strain results that are presented here indicate that the ISDG is measuring elastoplastic strains with good fidelity.

4 Computation of Stresses

The computation of stresses from the measured strains are based on the incremental J_2-flow theory:

$$\dot{e}_{ij} = \dot{S}_{ij}/2G + f(\sigma_e)\,\dot{\sigma}_e S_{ij} \tag{2}$$

where "$\cdot$" denotes an increment in the applied stresses and strains. The deviator stresses and strains are defined by $S_{ij} = \sigma_{ij} - 1/3\ \sigma_{kk}\delta_{ij}$ and $e_{ij} = \epsilon_{ij} - 1/3\ \epsilon_{kk}\ \delta_{ij}$. σ_{ij} and ϵ_{ij} are the stress and total strain components, respectively. The effective stress, σ_e, is given by $(3/2\ S_{ij}S_{ij})^{1/2}$.

The function $f(\sigma_e)$ describes the deviation of the material's effective stress-strain behavior from linear elasticity, and is equal to $3/2\ (1/E_t - 1/E)/\sigma_e$. The modulus of elasticity is of course E, and E_t is the slope, $d\sigma_e/d\epsilon$, of the effective-stress versus total-strain, ϵ, curve of the point of interest (this stress-strain curve is obtained in a uniaxial stress test).

Equation (2) can be contracted with S_{ij} to permit one to solve for $\dot{\sigma}_e$ by noting that $2\sigma_e\dot{\sigma}_e = 3S_{ij}\dot{S}_{ij}$. The effective stress increment, $\dot{\sigma}_e$, can then be re-inserted into Eq. (2) to produce an equation relating $\dot{S}_{ij}$ to $\dot{e}_{ij}$.

$$\dot{S}_{ij} = 2G\dot{e}_{ij} - FS_{ij}S_{kl}\dot{e}_{kl} \tag{3}$$

where

$$F = \frac{6Gf(\sigma_e)}{\sigma_e/G + 2\sigma_e^2 f(\sigma_e)}.$$

The total strain is made up of elastic and plastic components; i.e., $\epsilon_{ij} = \epsilon^e_{ij} + \epsilon^p_{ij}$. By noting that $\dot{\epsilon}^p_{kk} = 0$, one can finally write

$$\dot{\sigma}_{ij} = \alpha\dot{\epsilon}_{ij} + \beta\dot{\epsilon}_{kk}\delta_{ij} - FS_{kl}\dot{\epsilon}_{klk}S_{ij}. \tag{4}$$

$\alpha = 2G$, and $\beta = K - 2G/3$ where G and K have the familiar definitions from elasticity of $E/2\ (1+\nu)$ and $E/3(1-2\nu)$, respectively. Equation (4) relates the increments of stress to the increments of strain and is the constitutive expression used to compute the stresses from the measured strains.

The stress and strain state of interest here is one of plane stress on the surface at the root of the notch. The measurements are in the principal directions because of the symmetry at the center of the notch root. The principal stresses and strains are therefore labelled σ_1, σ_2, ϵ_1, ϵ_2, and ϵ_3, respectively. ϵ_1 and ϵ_2 are the strains that are measured, and the three unknowns can be solved from the three equations of (4). The final version of the equations that is used becomes:

$$\Delta\epsilon_3 = \frac{(FS_1S_3 - \beta)\Delta\epsilon_1 + (FS_2S_3 - \beta)\Delta\epsilon_2}{\alpha + \beta - FS_3^2} \tag{5}$$

$$\Delta\sigma_1 = (\alpha + \beta - FS_1^2)\Delta\epsilon_1 + (\beta - FS_1S_2)\Delta\epsilon_2 + (\beta - FS_1S_3)\Delta\epsilon_3 \tag{6}$$

$$\Delta\sigma_2 = (\beta - FS_1S_2)\Delta\epsilon_1 + (\alpha + \beta - FS_2^2)\Delta\epsilon_2 + (\beta - FS_2S_3)\Delta\epsilon_3. \tag{7}$$

The principal stress, σ_1 and σ_2, are the sums of the stress increments as computed from the above three equations.

Implementation of Eqs. (5)–(7) is straightforward. One has the experimental record of applied load, P, ϵ_1, and ϵ_2 stored as discrete points in a data file. At a given P_n, the strain increments are taken as $\epsilon_{n+1} - \epsilon_n$. The two stress increments are then computed and added to the stress values (computed previously) corresponding to P_n. However, there are a couple of points to be considered.

First, σ_e appears in the denominator of F in Eq. (3) so the computations have to be started in some manner. They are started by computing elastic stresses directly from the measured strains. σ_e is computed at every increment, and when it exceeds a present value, the program switches to the incremental calculations of Eqs. (5)–(7). This present value must be below the proportional limit of the material, and in practice, is taken as approximately 25 percent of the yield stress.

Second, the computation of $f(\sigma_e)$ involves $1/E_t$ which equals $d\epsilon/d\sigma$. Two kinds of 2024 aluminum were tested—T3 and T351. The Ramberg-Osgood representation of the stress-strain curve, $\epsilon = \sigma_e/E + (\sigma_e/M)^{1/n}$, fits the T351 stress-strain curve quite well, and $d\epsilon/d\sigma_e$ is easily computed. However, a much better fit to the uniaxial stress-strain curve for the T3 material is obtained with a polynomial, $\sigma_e = g(\epsilon)$, where $\epsilon = \sigma_e/E + \epsilon^p$. The effective plastic strain, ϵ^p, is the sum of the plastic strain increments defined by

$$\Delta\epsilon^p = \sqrt{2}/3[(\Delta\epsilon_1^p - \Delta\epsilon_2^p)^2 + (\Delta\epsilon_2^p - \Delta\epsilon_3^p)^2 + (\Delta\epsilon_1^p - \Delta\epsilon_1^p)^2]^{1/2}. \tag{8}$$

After the stress increments have been computed for load P_n, they are used to compute increments of elastic strain which are subtracted from the measured strain increments, $\Delta\epsilon_1$ and $\Delta\epsilon_2$, and the computed strain increment, $\Delta\epsilon_3$, to give the three plastic strain increments needed in Eq. (8). The effective plastic strain increment, $\Delta\epsilon^p$, is added to the previously computed ϵ^p

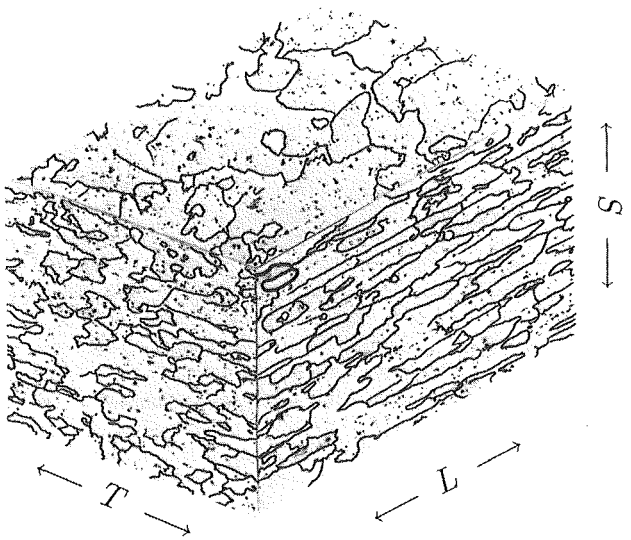

Fig. 2 Montage of photomicrographs of 2024 aluminum sheet—courtesy of Dr. J. C. Newman, Jr. The thickness of the grains in the S direction is approximately 25 micrometers. Grain boundaries have been highlighted.

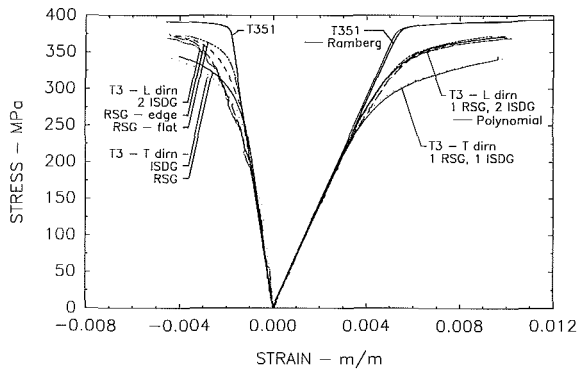

Fig. 3 Biaxial stress-strain curves from smooth specimens for the T3 and T351 materials. Measurements were made with the ISDG on the edge and with foil gages (RSG) on the flat side of the specimens. One lateral strain measurement was made on an edge with a RSG. The T3 material was tested both parallel (L) and perpendicular (T) to the rolling direction.

so that the proper value of ϵ is used for the calculation of E_t at P_{n+1}.

These computations are implemented in a short FORTRAN program on the same IBM-compatible microcomputer that was used for control of the experiments. Noise in the data does not appear to cause difficulties as will be seen in the next sections.

5 Material Response and Prediction for Smooth Specimens

This section presents the stresses and biaxial strains measured in uniaxial stress tests on smooth specimens. The purposes of these tests were to generate the constitutive equations needed for stress computation and to obtain biaxial strain data which could be used to check the computational procedures. One should be able to take the biaxial data, run it through the stress computation procedures, and get the result that $\sigma_1 = P/A$ and $\sigma_2 = 0$. As will be seen, the anisotropy of the material causes less than perfect agreement.

Figure 2 is a photomicrograph of 2024 sheet material showing the grain structure on the flat side of a sheet and on the edges; one edge parallel to the rolling direction, and one edge perpendicular to it. The nomenclature there is from ASTM E-399; "L" refers to the rolling direction, "T" to the width direction, and "S" to the edge direction. The grains have, in

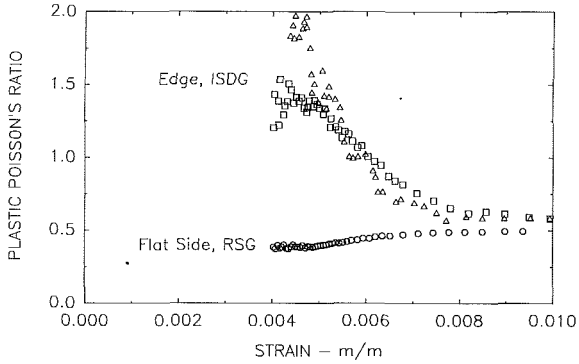

Fig. 4 The negative ratio of lateral and longitudinal plastic strain versus *longitudinal strain. The data presented are from* two smooth specimens that were instrumented with the biaxial ISDG on an edge and a smooth specimen with a biaxial RSG on the flat side.

general, the shape of elongated pancakes and are thinner in the direction perpendicular to the sheet.

Figure 3 shows the results from tests on three smooth specimens of 2024-T3 aluminum. One specimen was loaded in the L direction; it was instrumented with biaxial foil gages (RSGs) on the flat side and the biaxial ISDG on the edge. Another specimen was instrumented in the same way, but loaded in the T direction. A third specimen was loaded in the L direction, but used only the biaxial ISDG on the edge. In all cases, the agreement between the ISDG and the foil gage was excellent in the longitudinal direction (parallel to the load axis). But there is a significant difference between the lateral plastic strains measured on the flat side of a specimen with a foil gage and on the edge with the ISDG. That difference is greater when a specimen is loaded in the L direction than when one is loaded in the T direction.

It appears that the anisotropy of the material accounts for these differences in the lateral strains measured on the flat sides and edges of the smooth specimens. One might also argue that the indentations of the ISDG are influencing the plastic flow of the smaller grains on the edge. An argument against that hypothesis is that the agreement between the ISDG and the RSG lateral strains for the T-loaded specimen is actually fairly good. Also, if the indentations harden the specimen locally, one would expect smaller strains—not larger. Another test was run with a 0.79-mm long foil gage on the 2.5-mm thick edge of an L-loaded specimen. That result (RSG edge) is seen in Fig. 3 to lie between the edge lateral strains measured with the ISDG and the flat-side lateral strains. It therefore appears that the lateral ISDG-measured strains are reasonably accurate.

The 2024-T351 aluminum has the same general structure as the T3, but the grains are thicker in the S direction. The biaxial stress-strain curves, as measured with foil gages on the flat side and the edge of the smooth specimen, are nearly identical. One such curve is plotted in Fig. 3 and shows that this material is nearly elastic-perfectly plastic.

A representation of the uniaxial material behavior (actually the effective stress σ_e versus the total strain) is needed in order to evaluate $f(\sigma_e)$ in Eq. (3). The solid line through the "L" longitudinal strain data in Fig. 3 is a sixth-order polynomial fitted with the plotting package SIGMAPLOT from Jandel Scientific, Inc. Attempts to fit a Ramberg-Osgood equation to the data gave significant discrepancies either just after the proportional limit or at the maximum stress value and were abandoned. The equation describing the uniaxial stress-strain curve of 2024-T3 is:

$$\sigma = -0.4569 + 7.5004\times 10^4\epsilon - 5.5733\times 10^6\epsilon^2 + 3.6417\times 10^9\epsilon^3 - 1.0216\times 10^{12}\epsilon^4 + 1.0241\times 10^{14}\epsilon^5 - 3.4879\times 10^{15}\epsilon^6 \quad (9)$$

where σ is in MPa and ϵ is in m/m. The solid line fitted to the

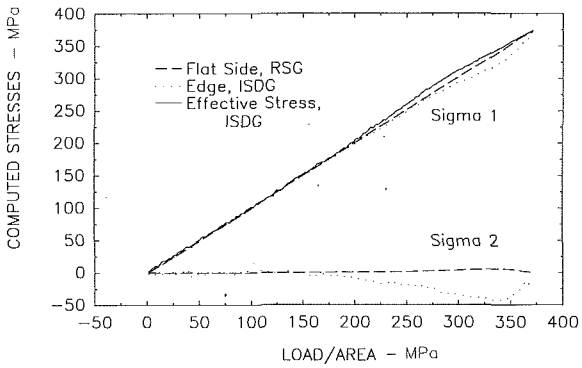

Fig. 5 Computed stresses for a smooth specimen versus the applied stress. The two principal stresses are computed from biaxial strains measured with foil gages on the flat side and the ISDG on the edge of the same specimen. The effective stress is computed only for the ISDG-measured stresses.

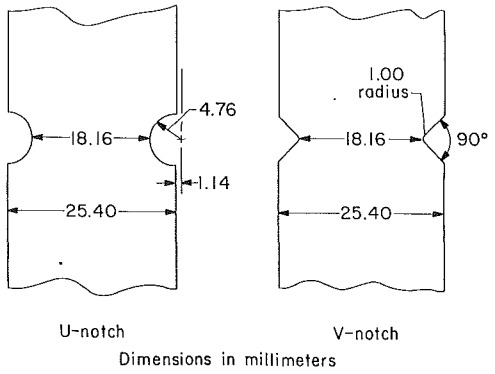

Fig. 6 Dimensions of the two types of notches

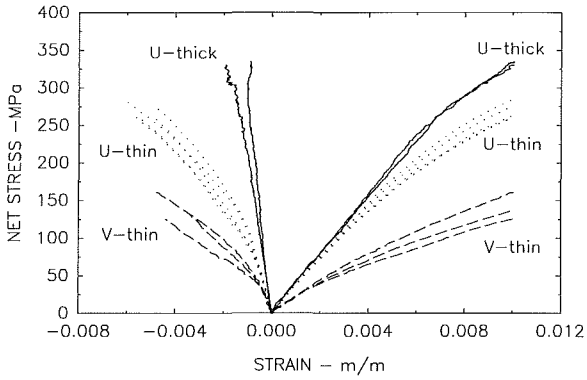

Fig. 7 Measured biaxial strains at the notch roots—longitudinal on the right and lateral on the left—for the three cases tested. The ordinate is the net stress applied to the specimen.

2024-T351 data is the Ramberg-Osgood equation with M = 414 MPa and n = 0.0094. This equation is much better at fitting a curve that has a sharper transition to plasticity.

The anisotropy considerations are important because J_2-flow theory assumes isotropy and that the plastic Poisson's ratio is 0.5. The anisotropy of the material is further illustrated in Fig. 4 which is a plot of the negative ratio of lateral to longitudinal plastic strain for the two specimens loaded in the L direction. The plastic strain was obtained by subtracting the computed elastic strain using $E = 71.8 \times 10^3$ MPa and $\nu = 0.325$. This subtraction and division generates noisy results at smaller strains, so the values are only plotted for longitudinal strains greater than 0.004 which corresponds roughly to the proportional limit of the material. The Poisson's ratio on the flat side of the specimen generally adheres to the assumption of the theory, but the edge results do not until later in the plastic yielding. Therefore, one cannot expect the computed stresses on the edge of the specimen to be accurate. However, the inaccuracy can be evaluated by using the biaxial strains measured on the smooth specimens—the data in Fig. 3—to compute the stresses σ_1 and σ_2. The result should of course be $\sigma_2 = P/A$ and $\sigma_2 = 0$.

The stresses computed using the data from the T3 specimen that was tested in the L direction and instrumented with both the foil gages and the ISDG are plotted in Fig. 5. The agreement is nearly perfect for the strains measured on the flat side of the specimen where the behavior is more isotropic; σ_1 is almost exactly equal to P/A, and σ_2 is nearly 0. Stresses computed from the edge data are noisier because of the coarser resolution of the ISDG, and σ_2 shows significant negative stresses. These clearly do not represent the physical situation; there are no compressive lateral forces in these long specimens to generate such a stress. The error in the computation comes from the deviation from isotropy in a direction perpendicular to the sheet material. Note that the computed edge stresses tend back toward perfect agreement at the higher stresses—the corresponding plastic Poisson's ratio of Fig. 4 tends toward 0.5 also.

In other words, the stresses computed from strains on the edge of the specimen (which are of greatest interest here) are simply incorrect. But, what is the effect of this error? The effective stress in this two-dimensional stress field is given by $(\sigma_1^2 - \sigma_1\sigma_2 + \sigma_2^2)^{1/2}$ which means that an error in σ_2 is suppressed. The effective stress computed from the edge stresses is plotted in Fig. 5 and agrees reasonably well with P/A; the maximum error is about five percent.

Based on these results, one can go ahead with the measurement of stresses at notch roots in this material with the understanding that the lateral stresses will be inaccurate, but the computed longitudinal stresses and the effective stresses will be accurate within ± five percent.

Table 1

Notch Thickness Shape	SCF Peterson	SCF FEM	SCF Measured	$(-\epsilon_x/\epsilon_y)_{el}$	Number of Tests
U-notch 2.5 mm	1.92	2.02	1.97	0.30	5
V-notch 2.5 mm	3.50	3.64	3.52	0.21	3
U-notch 25.4 mm	1.92	2.09	1.85	0.16	2

6 Biaxial Strain Results for Notched Specimens

Double-notched specimens were prepared with three different constraints at the notch root; i.e., three ratios of thickness to root radius. Two notch radii were used, and their dimensions are given in Fig. 6. Table 1 lists the three cases and their elastic stress concentration and constraint factors.

The "SCF Peterson" is a two-dimensional value from his handbook (Peterson, 1974). The "SCF FEM" are the results of a three-dimensional finite element analysis of the three geometries. The initial linear regions of the load versus longitudinal strain at the notch root were used to compute the "SCF Measured" value. Five tests were run for the thin U-notch geometry, and the variation of their initial slopes from the mean value was −2.4 percent + 5.7 percent which is an indicator of the fidelity of the ISDG measurement system.

The value $(-\epsilon_x/\epsilon_y)_{el}$ in Table 1 is the negative ratio of lateral to longitudinal elastic strain as calculated at the notch root in the finite element analysis. It should be the elastic Poisson's ratio of 0.325 for plane stress, and one sees that it is close to that value for the thin U-notch specimens. The sharper the stress concentration and the thicker the specimen, the smaller this value. It would be 0.0 for plane strain, but that would be very difficult to achieve without biaxial loading.

Figure 7 shows the results from ten different specimens for the three cases of Table 1. Each test was loaded in tension, and the testing program was set up so that when the longi-

tudinal strain reached a value of 0.01, the loading reversed. This value was chosen because cyclic loading over a range of ± 0.01 will produce microcracking at the notch root in a few hundred cycles. As mentioned earlier, the strain data used here is the monotonic part of a cyclic load sequence. The data sets ranged from 500 to 1000 points, but were reduced to around 150 for ease in plotting.

A notable feature of the data of Fig. 7 is the variation among the measured strains for a given case once the elastic limit has been passed. This is not at all surprising in view of the fact that the gage length is the same order of magnitude as the grain size of the aluminum. There is more variation among plastic strains for the V-notch specimens; the gage length there is 150 μm as opposed to 200 μm for the U-notch specimens. Part of this variation may come from local rotation of an indentation in a single grain or from plastic deformation of one of the faces of an indent. No matter what technique is used, measurement of plastic deformation over a few grains is likely to be inhomogeneous.

Figure 7 is the complete data set upon which the following stress computations are based. The variation among the plastic strains measured for supposedly identical specimens will of course show up in the computed stresses.

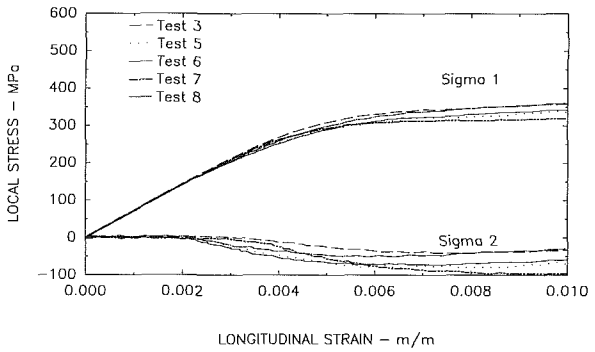

Fig. 8 Computed notch-root stresses for the thin U-notched specimens

7 Computed Notch-Root Stresses

Given the measured biaxial strains of Fig. 7 and Eqs. (5)–(7), the computation of the stresses is straightforward. The following three figures present the computed stresses for the three cases; they are plotted on the same scales. The abscissa is the measured longitudinal strain, ϵ_1; its upper limit of .01 was the same in all tests.

Figure 8 shows the stresses for the five U-thin specimens. The variation among the computed, σ_1 and σ_2 is similar to the variation among the measured ϵ_1 and measured ϵ_2, respectively. After all, ϵ_1 is the major contributor in the calculation of σ_1. The lateral stresses, σ_2, should be nearly zero in this thin specimen with a moderate stress concentration. They are negative—following the same pattern as the computed lateral stresses in the smooth specimens (see Fig. 5). This arises from the anisotropy of the material and again illustrates the point that the computed stresses are not completely correct.

The computed stresses for the V-thin specimens are shown in Fig. 9. The lateral stresses are approximately zero throughout the loading, but one can speculate that they should be a bit positive. That would be consistent with the increased level of constraint for this geometry as shown in Table 1.

The lateral stresses for the thick 2024-T351 specimens, as shown in Fig. 10, are always positive at the center of the notch root because of the greater constraint of the surrounding elastic material. The differences in the notch-root stresses for increasing constraint are clearly demonstrated in Figs. 8–10.

8 Comparison With the Neuber Prediction

The Neuber relation was derived using the deformation theory of plasticity for shear loading. Over the years, it has come to be used for cyclic loading of specimens or components

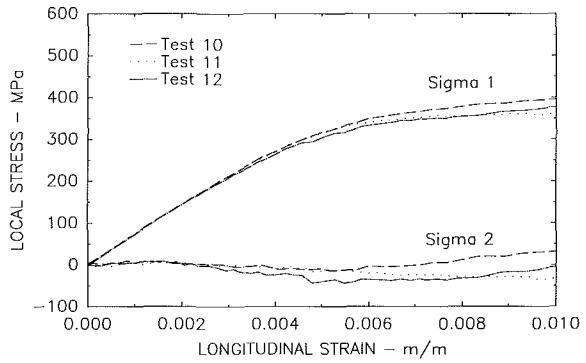

Fig. 9 Computed notch-root stresses for the thin V-notched specimens

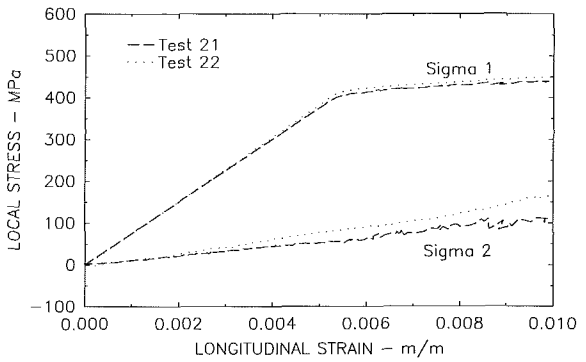

Fig. 10 Computed notch-root stresses for the thick U-notched specimens

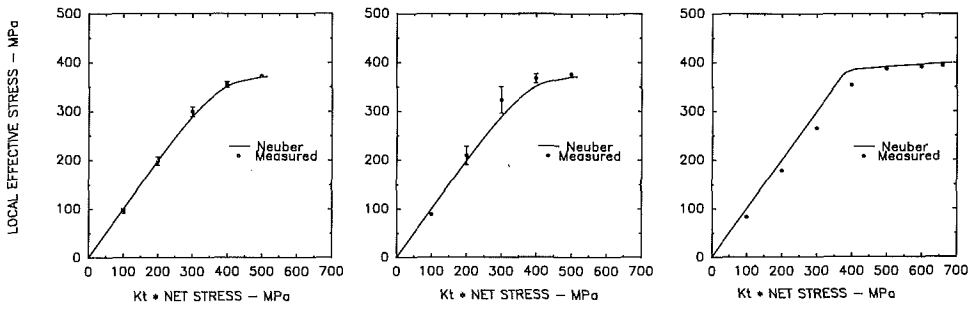

Fig. 11 Measured effective stresses at the notch root for the three cases and comparison with the predictions of the Neuber relation. (*a*) U-thin; (*b*) V-thin; (*c*) U-thick.

subjected to tensile or compressive loading. Certainly its simplicity has contributed to its popularity, but it is generally regarded to give accurate predictions of local stresses and strains only for plane-stress loading. The overall objective of the larger cyclic testing program (of which these monotonic results are a part) is to evaluate the Neuber relation for notched specimens with various amounts of constraint.

The computed stresses for the specimen with most constraint show significant positive lateral stresses at the notch root and lead one to use the effective stress, σ_e, as a measure of yielding. The Neuber relation does not recognize this; it predicts a single stress, σ_1, based on a uniaxial stress-strain curve (of course, this is σ_e if the stress at the notch root is truly uniaxial). It is therefore more appropriate to compare the measured effective stress with the Neuber-predicted stress, and this is done in Fig. 11.

Figure 11 is a plot of the local effective stress versus the product of the elastic stress concentration factor and the net stress; this latter quantity would be known by a designer seeking to predict the notch-root stresses. The Neuber prediction is a straightforward application of Eq. (1) and the appropriate constitutive equation. The experimental results shown were obtained by computing σ_e for each test at discrete values of $K_t \times \sigma_{net}$. Mean values were computed and are plotted as circles. The error bars represent the maximum and minimum values; not a statistical parameter. Where error bars are not visible, they were smaller than the size of the circle.

Figure 11 (a) shows near-perfect agreement between the predicted and measured effective stresses. This is for a moderate stress concentration factor and a thin specimen—nearly a purely plane-stress situation as shown in Table 1. Note that the agreement would not be as good if one used the measured σ_1. The average maximum value of σ_1 is 345 MPa (see Fig. 8), whereas the average maximum σ_e is 373 MPa—an eight percent difference. But, referring back to Fig. 5, σ_e is a better measure of the stress state in a smooth specimen. This result is nothing new; it was stated in the Introduction that the Neuber relation was generally valid for plane stress.

Figures 11 (b) and 11 (c) show a greater discrepancy as one moves toward more constraint, but in each case the peak σ_e agree very closely. It is also interesting to note that the scatter among the peak values of σ_e is very small for all three cases—in spite of the scatter in the measured strains and the computed stresses. The stress-strain curves flatten beyond the yield point, and therefore large strain errors produce only small stress errors.

9 Conclusions

There are three main conclusions from this work:

- Biaxial elastoplastic strain measurements are feasible over short gage lengths in materials and geometries that have practical significance. When applied to geometries that dictate the principal strains and materials that meet the assumptions of the theory, the addition of a second strain component enables one to compute stresses. Although the ISDG measurement system is somewhat sophisticated, once it is set up, testing becomes routine. The strain measurements demonstrate the needed for replication when plastic strains are measured over gage lengths on the order of the grain size. However, the variability among the strains is suppressed when they are used to compute effective stresses.
- Computation of elastoplastic stresses from measured strains is easy—given modern microcomputer-based measurement systems. The lack of accuracy lies more in the representation of the material's constitutive behavior than in the strain measurements and the computational procedures. Anisotropy of the material is important and leads to moderate errors in the longitudinal stress, σ_1, but large errors in the lateral stress, σ_2. That is not a fatal flaw because one is really more interested in the effective stress which suppresses the error in σ_2.
- The results show that the predicted peak stress from the Neuber relation agrees with the measured peak effective stress within the startling range of ± two percent! The Neuber relation is a good predictor of the effective stress at a notch root for monotonic loading regardless of the amount of constraint. This is important because a stress-based plasticity criterion should use the effective stress. However, it does not follow that the Neuber relation gives a good prediction of the strains; the shape of the upper portion of the stress-strain curve tends to dampen the variation of stresses. Low-cycle fatigue predictions are based on strain-life curves, so this point is important. However, for static design and monotonic loading, these results give one considerable confidence in the Neuber relation.

It is hoped that this presentation of the measured biaxial strains and the resulting computed stresses will contribute to a better understanding of the basic mechanics of notch-root behavior. The longer term goal is to gain a better understanding of the initiation phase of fatigue crack growth in order to improve life predictions.

Acknowledgments

The author appreciates the support of this research by the National Science Foundation under Grant MSM-8702110. It is part of a larger program to develop biaxial strain measurement techniques and use them to study cyclic plasticity under low-cycle fatigue conditions. The monotonic biaxial strain data is taken from the Ph.D. thesis of Dr. K. C. Wang; his careful work in measuring cyclic biaxial strains is an important contribution. Most of the preparation of this paper was done while the author was a Research Associate at NASA-Langley; the support of the National Research Council for that period is appreciated.

References

Durelli, A. J., and Sciammarella, C. A., 1963, "Elastoplastic Stress and Strain Distribution in a Finite Plate with a Circular Hole Subjected to Unidirectional Load," ASME Journal of Applied Mechanics, Vol. 30, pp. 115–121.

Griffith, G. E., 1948, "Experimental Investigation of the Effects of Plastic Flow in a Tension Panel with a Circular Hole," NACA-TN 1705.

Guillot, M. W., and Sharpe, Jr., W. N., 1983, "A Technique for Cyclic-plastic Notch-strain Measurement," *Experimental Mechanics*, Vol. 23, pp. 354–360.

Johnson, R. L., 1976, "Measurement of Elastic-Plastic Stresses by Scattered-light Photomechanics," *Experimental Mechanics*, Vol. 16, pp. 201–208.

Keil, S., and Benning, O., 1979, "On the Evaluation of Elasto-Plastic Strains Measured with Strain Gages," *Experimental Mechanics*, Vol. 19, pp. 265–270.

Kobayashi, A. S., ed., 1987, *Handbook on Experimental Mechanics*, Prentice-Hall, Englewood Cliffs, N.J., pp. 8–10.

McClintock, F. A., 1963, Discussion of "Experimental Solution of Elastic-Plastic Plane-Stress Problems," ASME Journal of Applied Mechanics, Vol. 30, pp. 631–634.

Neuber, H., 1961, "Theory of Stress Concentration for Shear-Strained Prismatical Bodies With Arbitrary Nonlinear Stress-Strain Law," ASME Journal of Applied Mechanics, Vol. 28, pp. 544–550.

Peterson, R. E., 1974, *Stress Concentration Factors*, John Wiley and Sons, New York.

Sharpe, W. N., Jr., and Wang, K. C., 1991, "Evaluation of a Modified Neuber Relation," *ASME Journal of Engineering Materials and Technology*, Vol. 113, pp. 1–8.

Sharpe, W. N., Jr., 1982, "Applications of the Interferometric Strain/Displacement Gage," *Optical Engineering*, Vol. 21, pp. 483–488.

Theocaris, P. S., 1962, "Experimental Solution of Elastic-Plastic Plane-Stress Problems," ASME Journal of Applied Mechanics, Vol. 29, pp. 735–743.